Int J Adv Manuf Technol (2013) 69:583–593
DOI 10.1007/s00170-013-5048-0

ORIGINAL ARTICLE

An improved surface roughness measurement method for micro-heterogeneous texture in deep hole based on gray-level co-occurrence matrix and support vector machine

Wei Liu · Xianming Tu · Zhenyuan Jia · Wenqiang Wang · Xin Ma · Xiaodan Bi

Received: 7 December 2012 / Accepted: 29 April 2013 / Published online: 19 May 2013

Abstract Microscopic vision system has been employed to measure the surface roughness of micro-heterogeneous texture in deep hole, by virtue of frequency domain features of microscopic image and back-propagation artificial neural network optimized by genetic algorithm. However, the measurement accuracy needs to be improved for engineering application. In this paper, we propose an improved method based on microscopic vision to detect the surface roughness of R-surface in the valve. Firstly, the measurement system for the roughness of R-surface in deep hole is described. Thereafter, the surface topography images of R-surface are analyzed by the gray-level co-occurrence matrix (GLCM) method, and several features of microscopic image, which are nearly monotonic with the surface roughness, are extracted to fabricate the prediction model of the roughness of R-surface accurately. Moreover, a support vector machine (SVM) model is presented to describe the relationship of GLCM features and the actual surface roughness. Finally, experiments on measuring the surface roughness are conducted, and the experimental results indicate that the GLCM-SVM model exhibits higher accuracy and generalization ability for evaluating the microcosmic surface roughness of micro-heterogeneous texture in deep hole.

Keywords Surface roughness · Gray-level co-occurrence · Textural analysis · Genetic algorithm · SVM algorithm · Micro-heterogeneous texture

W. Liu (✉) · X. Tu · Z. Jia · W. Wang · X. Ma · X. Bi
Key Laboratory for Precision and Non-traditional Machining Technology of the Ministry of Education, School of Mechanical Engineering, Dalian University of Technology, 2 Lingong Road, Dalian 116024, China
e-mail: lw2007@dlut.edu.cn

1 Introduction

Surface roughness is one of the important parameters for evaluating the surface quality of the part, which has a direct impact on the serving performance of the part, especially for the sealing surface in deep hole of valve. In order to meet the requirements of the sealing performance under low-temperature circumstance, generally, the sealing structure in deep hole of valve is designed as the micro-heterogeneous structure. However, due to the measurement space constraint, the smaller feature size, and the higher machining accuracy, the roughness of the R-surface in deep hole of valve is difficult to detect. Therefore, a roughness measurement method of the R-surface in valve is urgent for assessing the surface quality of the micro-heterogeneous structure in deep-hole parts.

In recent years, the computer vision-based methods, which allow the roughness to be measured rapidly with high accuracy and flexibility, have attracted a great deal of attention from more researchers [1, 2]. The vision measurements of surface roughness are mainly fabricated by the extraction method of image features which can represent the surface roughness and the surface roughness estimation model. Generally, the texture analysis is considered as a basic and effective method in extracting the image features. The texture analysis algorithms are mainly composed of three categories: statistical method, structural method, and frequency domain-based method [3]. Tsai extracted the image features on the basis of frequency domain method to measure the surface roughness [4]. Lee proposed a method to assess surface roughness using statistical features of surface image [5]. Their results demonstrated the validity of the proposed approach to achieve accurate Ra values, although it was not stated how much acquired Ra values vary with light or material change. Hu developed a method to

evaluate 3D surface roughness based on statistical method, and the experimental data showed that mean of histogram, variance of histogram, and root-mean-square deviation of surface are increasing along with increasing Ra. However, they cannot generalize the exact correlation between the steeper parameter and Ra, which need further research [6]. In our past work, we selected Fourier transform (FT) to characterize surface roughness in the frequency domain [7]. However, FT methods usually perform well on textures showing strong periodicity. As the periodicity of textures weakens, their performance will deteriorate.

Gray-level co-occurrence matrix (GLCM), one of the most important texture analysis methods, has been widely used for image procedure in many applications. By virtue of an accurate GLCM technique, Dutta successfully detected the tool condition from the turned surface images [8]. Alegre extracted relevant information of the image by means of GLCM [9]. Gadelmawla selected four parameters obtained from GLCM as inputs to characterize surface roughness, and it was found that the proposed parameters had a good correlation with the average roughness [10]. Xian extracted five texture features: energy, contrast, correlation, entropy, and homogeneity by means of GLCM from the liver segmented images to classify liver disease [11]. The results demonstrated that GLCM texture technique was feasible and excellent in ultrasonography classification of liver tumor. Therefore, GLCM has exhibited the potential of recognizing the image features for roughness measurement.

Another problem is to establish an estimation model for surface roughness. The differential evolution algorithm-based artificial neural network was proposed to predict surface roughness in turning operations [12]. In our past work, the conventional neural network based-method has such disadvantages as over fitting on training data, leading to poor generalization ability and too long training time. Thus, in this paper, we employ a highly effective system modeling method, support vector machine (SVM). Based on statistical theory and risk minimization principle, SVM has proved to be able to give excellent performances in various applications [13, 14] and show a higher accuracy than neural network through experiments of performance comparison [15, 16]. Lela employed regression analysis, Bayesian neural network, and SVM as three methodologies to examine the influence of three cutting parameters on surface roughness, and results showed that all three methods were applicable in measuring surface roughness [17]. Ekici built SVM surface roughness prediction model for AISI 304 austenitic stainless steel in CNC turning operation based on three different SVM tools and artificial neural network (ANN). The experimental results showed that all results of SVM models were better than that of ANN with high correlations between the predicted values and experimentally measured ones [18].

In this paper, consequently, an improved roughness measurement method for R-surface in the valve is proposed, by employing GLCM and SVM algorithm. The measurement system is introduced briefly in Section 2. Thereafter, several features of microscopic image from GLCM are extracted to prepare the input data for the prediction model of the roughness of R-surface, as given in Section 3. Then, in Section 4, a SVM model is presented to describe the relationship of GLCM features and the actual surface roughness values. In Section 5, experimental results for the GLCM-SVM model, the back-propagation (BP) model, and the genetic algorithm–back-propagation (GA-BP) model are compared and analyzed. Conclusions are given in Section 6.

2 Measurement method and system

The improved surface roughness measurement method based on GLCM and SVM is proposed for micro-heterogeneous texture in deep hole, such as R-surface as shown in Fig. 1. Firstly, the microscopic images of R-surface of valve samples are obtained by using a large depth of field of a long working distance microscope. Moreover, GLCM method is employed to analyze and extract these image features, which show approximately monotonic relationship with surface roughness. Then, it is noticeable that enough actual roughness values of R-surface must be obtained to fabricate the database, which can represent the relationship between the features of R-surface and the actual surface roughness. Therefore, we have to employ some sample valves and cut away the sections of sample valve over R-surface, in order to get the actual roughness valves of R-surface by the surface profiler. Then, we establish a

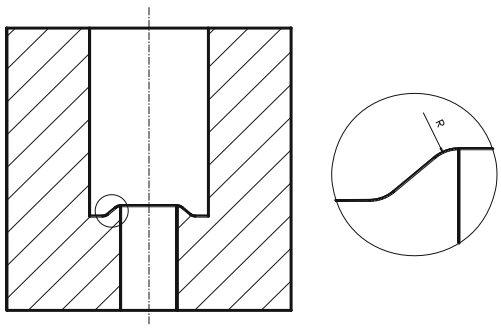

Fig. 1 The sealing R-surface of valves

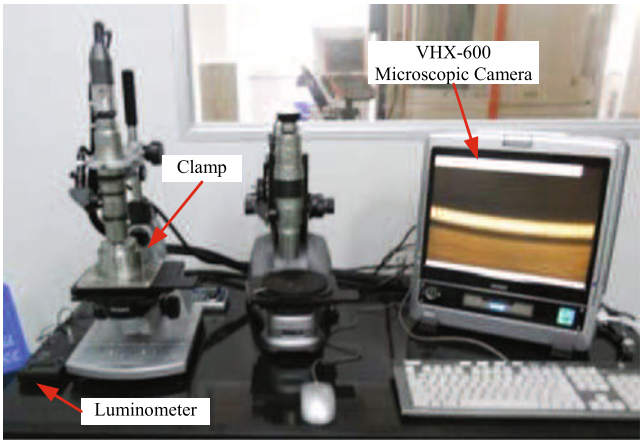

Fig. 2 The microscopic vision system for capturing the images of R-surface

SVM estimation model to predict other unknown surface roughness values of R-surface.

The roughness measurement system for R-surface in deep hole, as shown in Fig. 2, contains the vision system for capturing the microscopic images of R-surface and the calibration system for acquiring the actual roughness of R-surface. The microscopic image of R-surface, with 1,600 × 1,200 resolution, is captured by a digital microscopic camera with the long working distance lenses of 85 mm (VHX-600, Keyence). A ring light source is arranged to uniformly illuminate the R-surface, and a halogen lamp with a voltage of 12 V and a power of 100 W is applied in the display , which is transmitted by optical fiber to the digital microscopic camera. Moreover, in order to investigate the surface roughness of different sections of R-surface along the circumferential direction, we have designed a clamp system with a digital luminometer, which can quantify the light luminosity projected on the R-surface.

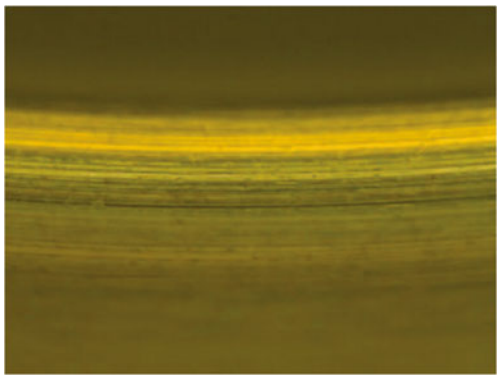

Fig. 3 The microscopic image of R-surface under the magnification of ×300

Figure 3 shows a microscopic image of R-surface in deep-hole valve under the magnification of ×300. It can be seen from Fig. 3 that the microscopic image captured by the proposed microscopic vision system is clear and suitable for image processing.

In order to fabricate the relationship data of the image features and the actual roughness of R-surface, the upper sections of some sample valves are machined and cut away at the position of 5 mm over the detected R-surface by EDM, and the roughness of R-surface can be measured by the 3D surface profiler (ZYGO NewView 5022, Fig. 4) with a calibration clamp, as shown in Fig. 5. The maximum vertical resolution of this 3D surface profiler can reach 0.1 nm and can fully meet the calibration requirements of R-surface.

Moreover, it is noticeable that the sampling length and the evaluation length of R-surface roughness based on traditional evaluation method of roughness cannot meet the measurement requirements, due to the small area and structure of R-surface. Therefore, according to ISO 25178 (Geometric Product Specifications) relating to the analysis of 3D areal surface texture, arithmetical mean height S_a is employed to evaluate the roughness of R-surface, which can be expressed by

$$S_a = \frac{1}{A}\int_A |z(x, y)|\, dxdy \tag{1}$$

where A is the sampling area and $z(x, y)$ is the deviation of arbitrary point from the datum plane. In addition, we will also employ the contour largest single-peak distance S_{max} as the filtering parameter to filter out the form error and waviness of R-surface [7].

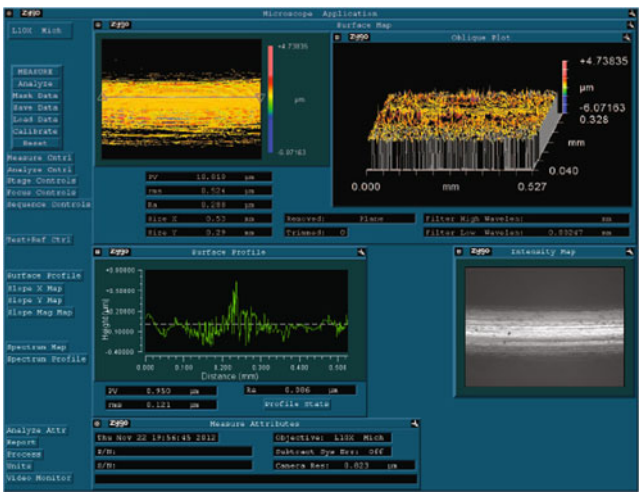

Fig. 4 The calculation of S_a using the 3D surface profiler

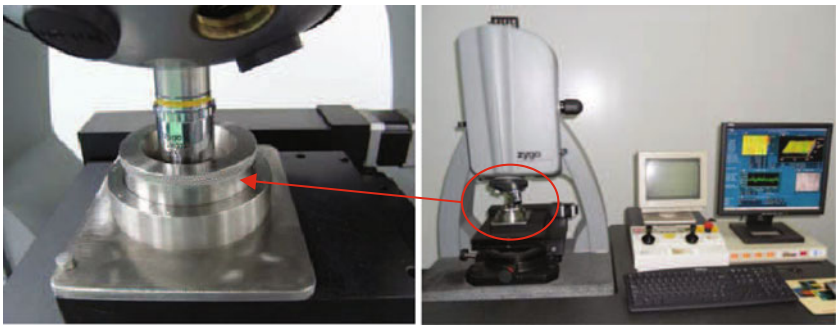

(a) (b)

Fig. 5 The calibration system (**b**) for acquiring the actual roughness of R-surface and the calibration clamp (**a**)

3 Extraction of microscopic image features

Any image can be viewed as a surface in 3D space, where the gray levels of two pixels with a certain distance are same or different. An appropriate method to find out the joint statistical distribution between the two pixels will facilitate to analyze the image texture. GLCM is such a method which describes the image texture by detecting the spatial correlation of the image and which reflects the integrated information of image gray on direction, adjacent interval, and amplitude.

The GLCM is defined as the joint probability distribution of two pixels with a distance on the image in mathematics. Detailed description is as follows: two different points in the image, (x, y) and $(x+a, y+b)$, have the gray level of (i, j). When the values of a and b are fixed, there will be various values (i, j) for the points (x, y) in the whole image. If the gray scale of the image is G , then the combination of i and j will be G^2. In the whole image, the occurrence number $P(i, j|d, \theta)$ for each value (i, j) is calculated; then, the GLCM $P(i, j|d, \theta)$ can be written by

$$P(i, j/d, \theta) = \#\{(x, y), (x+a, y+b)|f(x, y) = i, f(x+a, y+b) = j\} \quad (2)$$

where $i, j = 0, 1, \ldots, G-1$, x, y are the pixel coordinates in the image, d measured in number of pixels is the building step, θ is the building direction, whose value is usually 0°, 45°, 90°, and 135° as shown in Fig. 6.

Supposed that the gray scale G of the image is 8, the resolution of the image is 7×5, building direction and building step are 0° and 1, respectively. Then, the occurrence number $P\ (4, 3|1, 0°)$ equals to 3, which is calculated as shown in Fig. 7. Meanwhile, according to the definition of the building direction shown in Fig. 6, GLCM is a symmetric matrix.

3.1 Determination of constructing parameters

It can be seen from the definition of GLCM that the gray scale of the image, building direction, and building step are the key parameters which affect the size of GLCM. The GLCM features will be different under different combinations of different values of these three parameters, so is their description to the image texture. Consequently, appropriate constructing parameters should be selected before employing GLCM to analyze the microscopic image of R-surface.

1. Determination of gray scale

   The larger the G, the clearer the image will be and the more real the texture information will be. However, with the larger G, the size of GLCM will become larger, which induces an increase in the amount of computation. However, if the gray scale is compressed within a narrow range, the detail information of the image will be lost and feature extraction of the

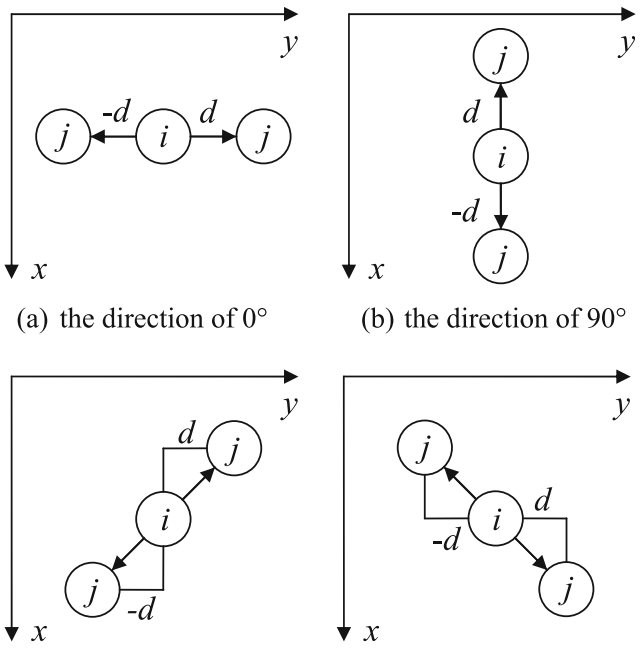

Fig. 6 The four building directions of GLCM

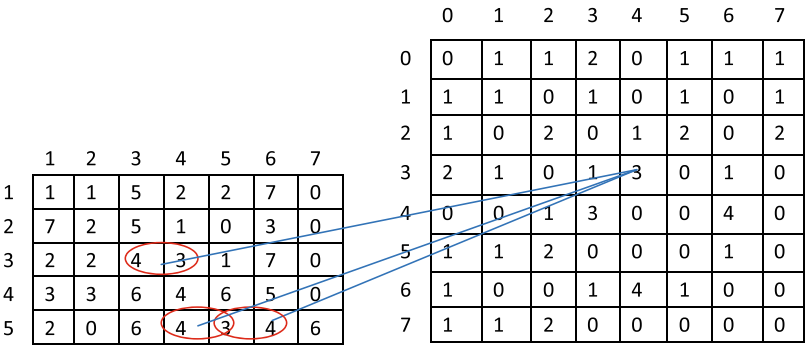

Fig. 7 The calculation process of GLCM

(a) The gray value distribution of the image (b) Gray level co-occurrence matrix (GLCM) for the image

microscopic image will be difficult. The main function of R-surface is to ensure the sealing performance of the valve, so the clearer image and the more textural information are important for estimating accurately the surface roughness and judging the sealing performance. Therefore, the gray scale of microscopic image of R-surface, with the G value of 256, will not be compressed in this paper.

2. Determination of building direction

   The building direction of GLCM of microscopic image is another important variable. For example, as shown in Table 1, feature parameters of GLCM are listed with the building direction of 0°, 45°, 90°, and 135° and the mean values in the four directions, the gray scale of 256, the building step d of 2, and the actual roughness value of 0.636 μm for a microscopic image of R-surface.

   As shown in Table 1, the feature parameters of GLCM in different building directions are quite different. Therefore, in order to prevent from losing the image textural information in any direction, the average value of feature parameters in the four directions is employed to calculate the GLCM features.

3. Determination of building step

   Figures 8 and 9 show the relationship curves between the GLCM features and the building step with different actual surface roughness values, with the gray scale of 256 and the average value of feature parameters in the four directions. Due to the limitation of the paper length, only the curves of correlation and angle of second-order moment are listed in Figs. 8 and 9, respectively. As shown in Figs. 8 and 9, the GLCM feature parameters can be employed to distinguish the different surface roughness of R-surface, when the building step d is selected by 2 or 3. However, some pixels cannot participate into calculating GLCM with a larger building step, which induces the loss of some image details. Consequently, the building step d is selected by 2.

3.2 Feature extraction of microscopic image of R-surface

Generally, the secondary statistics from the obtained GLCM is employed to describe the image texture more intuitively in the practical application. Moreover, before feature extraction of R-surface image, the normalized matrix $\hat{P}(i, j|d, \theta)$ (abbreviated as $\hat{P}(i, j)$) of GLCM $P(i, j|d, \theta)$ is necessary for facilitating to analyze the features of microscopic image of R-surface:

$$\hat{P}(i, j) = \hat{P}(i, j|d, \theta) = P(i, j|d, \theta)/R \tag{3}$$

where R is the sum of elements in the gray-level co-occurrence matrix.

In this paper, we select six features from the normalized matrix $\hat{P}(i, j|d, \theta)$, which show approximately monotonic relationship with respect to the actual surface roughness

Table 1 Features in different directions

Direction	Correlation	Differential entropy	Angle of second-order moment	Inverse gap	Maximum probability	Sum of variance
0°	0.993061	0.788566	0.001639	0.494802	0.004976	2,378.125
45°	0.909997	1.330037	0.000399	0.223766	0.001347	2,291.17
90°	0.916216	1.314826	0.000413	0.229236	0.001399	2,298.628
135°	0.912489	1.325735	0.000402	0.225341	0.001429	2,294.171
Mean	0.932941	1.189791	0.000713	0.293287	0.002288	2,315.523

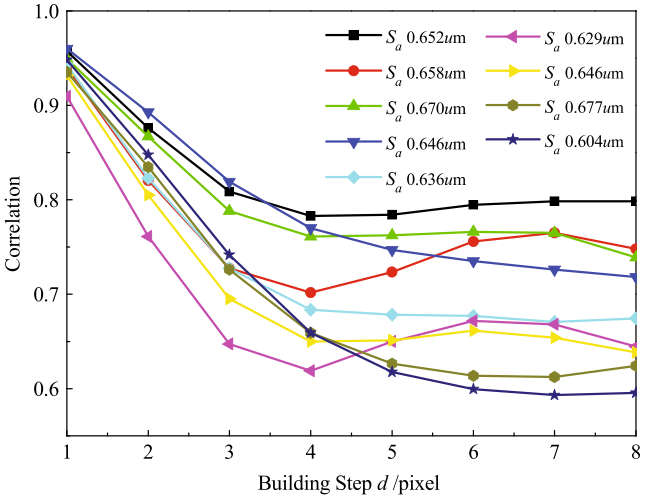

Fig. 8 Correlation changes under different building step with different S_a values

values of R-surface. The quantitative definitions of these features are given below:

1. Correlation

$$F_1 = \frac{\sum_{i=0}^{G-1}\sum_{j=0}^{G-1}(i-\mu_x)(j-\mu_y)\hat{P}(i,j)}{\sigma_x\sigma_y} \tag{4}$$

where $u_x = \sum_{i=0}^{G-1} i \sum_{j=0}^{G-1}\hat{P}(i,j)$, $u_y = \sum_{j=0}^{G-1} j \sum_{i=0}^{G-1}\hat{P}(i,j)$, $\sigma_x = \sum_{i=0}^{G-1}(i-u_x)^2\sum_{j=0}^{G-1}\hat{P}(i,j)$, $\sigma_y = \sum_{j=0}^{G-1}(j-u_y)^2\sum_{i=0}^{G-1}\hat{P}(i,j)$.

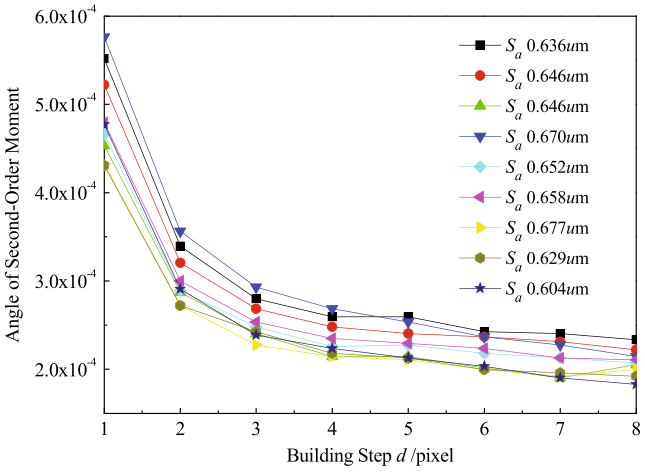

Fig. 9 Angle of second-order moment changes under different building step with different S_a values

Correlation is used to measure the similar degree of the GLCM element in a row or column. If the image has a stronger texture in the θ direction and a weaker one in the other directions, then the value of F_3 in the θ direction will be significantly bigger than the ones in the other directions. As shown in Fig. 3, the image has a stronger texture in the direction of 0°. Thus, correlation in the direction of 0° is the biggest.

2. Differential entropy

$$F_2 = -\sum_{k=0}^{G-1}\sum_{i=0}^{G-1}\sum_{j=0}^{G-1}\hat{P}(i,j)\times\log\left[\sum_{i=0}^{G-1}\sum_{j=0}^{G-1}\hat{P}(i,j)\right] \tag{5}$$

where $|i-j|=k$. Differential entropy represents the information of the image. It can measure the randomness of the image and distinguish the complexity of the texture.

3. Angle of second-order moment

$$F_3 = \sum_{i=0}^{G-1}\sum_{j=0}^{G-1}\hat{P}^2(i,j) \tag{6}$$

Angle of second-order moment is also called energy, which is the square of each element in the GLCM, and reflects the homogeneous degree of the gray-level distribution and thickness of the image texture.

4. Inverse gap

$$F_4 = \sum_{i=0}^{G-1}\sum_{j=0}^{G-1}\hat{P}(i,j)/\left[1+(i-j)^2\right] \tag{7}$$

Inverse gap is used to measure the local changes among the image textures. It reflects the regular extent of texture. The more regular the texture, the bigger F_4 will be.

5. Maximum probability

$$F_5 = \max_{i,j}\left[\hat{P}(i,j)\right] \tag{8}$$

6. Sum of variance

$$F_6 = \sum_{k=0}^{2G-2}(k-SA)^2 P_X(k) \tag{9}$$

where $SA = \sum_{k=0}^{2G-2} k \sum_{i=0}^{G-1}\sum_{j=0}^{G-1}\hat{P}(i,j)$ and $P_X(k)$ is a row vector with the dimension of $2G-1$. The first and second elements of the row are equal to zero and the other elements are equal to $\sum_{k=0}^{2G-2}\hat{P}(i,j)$, where $|i+j|=k$. Variance reflects the cycle of the texture. The bigger the F_6 value, the bigger is the cycle of texture.

Consequently, these selected six features cover all the aspects to describe the image texture and can represent the overall characteristics of the R-surface microscopic images.

4 Construction of roughness estimation model

4.1 The theory of SVM regression algorithm

The SVM proposed by Vapnik is known as an excellent tool for the classification and regression problems of good generalization ability, which is suitable to solve nonlinear regression estimation problems [19]. The core thought of SVM is to nonlinearly map the input data x to a higher dimensional feature space to yield and solve a linear regression problem in the feature space. Given a training sample set $G = \{x_i, y_i\}_i^k$, where x_i denotes the input vector, y_i denotes the actual value, and k denotes the total number, the SVM regression function is formulated as follows:

$$f(x) = \omega \cdot \varphi(x) + b \tag{10}$$

where ω is the weight vector, b is the scalar threshold, and $\varphi(x)$ is called the feature nonlinearly mapped from the input space x. Moreover, all training sample data can be error-free-fitted by the nonlinear function $f(x)$ under the ε precision :

$$\begin{cases} y_i - \omega \cdot \varphi(x_i) - b \le \varepsilon \\ \omega \cdot \varphi(x_i) + b - y_i \le \varepsilon \end{cases} i = 1, 2, \ldots, k \tag{11}$$

After the positive slack variables ξ_i and ξ_i^*, representing the distance from the actual values to the corresponding boundary values of ε insensitive, are introduced, the regression estimation problem can be transformed into minimization function:

$$\mathrm{Min} R\left(\omega, \xi_i^*, \xi_i\right) = \frac{1}{2}\|\omega\|^2 + C\sum_{i=1}^{k}\left(\xi_i + \xi_i^*\right) \tag{12}$$

subject to:

$$\begin{cases} y_i - \omega \cdot \varphi(x_i) - b \le \varepsilon + \xi_i \\ \omega \cdot \varphi(x_i) + b - y_i \le \varepsilon + \xi_i^* \\ \xi_i, \xi_i^* \ge 0 \end{cases} i = 1, 2, \ldots, k \tag{13}$$

where the first part $\|\omega\|^2/2$ measures the smoothness of the function applied to promote the generalization ability and the second part $C\sum_{i=1}^{k}\left(\xi_i + \xi_i^*\right)$ is called the penalty factor and is a positive number. The error can be neglected when the difference between $f(x_i)$ and y_i is less than ε. As the minimization of function (12) is a convex quadratic optimization problem, the local optimal solution is certainly the global optimal one, which can be solved by the introduction of Lagrangian function:

$$\begin{aligned} L(\omega, b, \xi, \xi^*, \alpha, \alpha^*, \gamma, \gamma^*) &= \frac{1}{2}\|\omega\|^2 + C\sum_{i=1}^{k}\left(\xi + \xi^*\right) \\ &- \sum_{i=1}^{k}\alpha_i\left(\xi_i + \varepsilon - y_i + \omega \cdot \varphi(x_i) + b\right) \\ &- \sum_{i=1}^{k}\alpha_i{}^*\left(\xi_i^* + \varepsilon + y_i - \omega \cdot \varphi(x_i) - b\right) \\ &- \sum_{i=1}^{k}\left(\xi_i\gamma_i + \xi_i^*\gamma_i{}^*\right) \end{aligned} \tag{14}$$

where α_i, $\alpha_i{}^*$, γ, and γ^* are Lagrange multiplier. The minimization of the Lagrangian function then can be converted to the so-called dual problem:

$$\begin{aligned} \mathrm{Max} Q\left(\alpha, \alpha^*\right) = &-\frac{1}{2}\sum_{i=1}^{k}\sum_{j=1}^{k}\left(\alpha_i - \alpha_i^*\right)\left(\alpha_j - \alpha_j^*\right)k(x_i, x_j) \\ &- \sum_{i=1}^{k}\left(\alpha_i + \alpha_i^*\right)\varepsilon + \sum_{i=1}^{k}\left(\alpha_i - \alpha_i^*\right)y_i \end{aligned} \tag{15}$$

subject to

$$\begin{cases} \sum_{i=1}^{k}\left(\alpha_i - \alpha_i^*\right) = 0 \\ 0 \le \alpha_i \le C \\ 0 \le \alpha_i^* \le C \end{cases}, i = 1, 2, \ldots, \tag{16}$$

where $k(x_i, x_j) = \varphi(x_i) \cdot \varphi(x_j) = \varphi(x_i)^T\varphi(x_j)$ is called the kernel function, and the value of the kernel equals the inner product of two vectors x_i and x_j in the feature space $\varphi(x_i)$ and $\varphi(x_j)$. The kernel function is intended to handle any dimension feature space without the need to calculate $\varphi(x)$ accurately. Consequently, the network output $f(x)$ then equals to the explicit form:

$$f(x) = \sum_{i=1}^{k}\left(\alpha_i - \alpha_i^*\right)k(x_i, x) + b\,. \tag{17}$$

4.2 Parameter setting of the SVM model

In the SVM model, the main parameters are kennel function, penalty factor C, and sensitive coefficient ε. The first thing to apply SVM is to choose the kennel function. It is noticeable that any function that can satisfy Mercer's condition can be used as the kernel function. As the relationships between the selected six parameters and the surface roughness are strongly nonlinear, in this paper, RBF kernel

function is selected as the kennel function, which generally can bring a better estimation performance.

The sensitive coefficient ε determines the margin within which the error is neglected. The smaller its value, the higher the accuracy of learning is required and more support vectors will be found by the algorithm. The regularization coefficient C is the weight, which determines the balance between the complexity of the network, characterized by the weight vector ω and the error of approximation, measured by the slack variables and the value of ε.

5 Experiment and analysis

5.1 SVM estimation model training

Firstly, in order to contrast the performance of the surface roughness estimation model, the evaluation criteria of mean absolute percentage error (MAPE), maximum relative error (MRE), maximum absolute error (MAE), and root-mean-square error (RMSE) are adopted:

$$\mathrm{MAPE} = \frac{1}{N}\sum_{i=1}^{N}\left|\frac{A_i - F_i}{A_i}\right| \tag{18}$$

$$\mathrm{MRE} = \max\left\{\left|\frac{A_i - F_i}{A_i}\right|\right\} \tag{19}$$

$$\mathrm{MAE} = \max\{|A_i - F_i|\} \tag{20}$$

$$\mathrm{RMSE} = \sqrt{\frac{1}{N}\sum_{i=1}^{N}(A_i - F_i)^2} \tag{21}$$

where A_i and F_i are the actual and predictive values, respectively, and N is the number of detected samples.

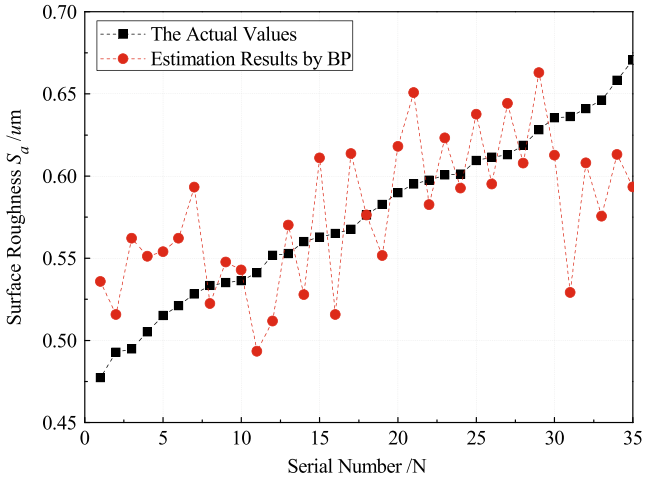

Fig. 10 Estimation results of the BP model

The selected GLCM statistical features are extracted from the obtained microscopic images. Besides, the actual surface roughness values of the corresponding position of R-surface in sample valves are detected by the 3D surface profiler, as shown in Fig. 5. Then, the statistical features of the microscopic images and their actual surface roughness value fabricate together the database, so as to establish the roughness estimation model based on the SVM algorithm. A portion of GLCM features and actual roughness values of R-surface in sample valves are listed in Table 2.

As shown in Table 2, the extracted image GLCM features of R-surface in sample valves are not within the same order of magnitude value. Then, normalization processing is necessary before training, but it is removed after training.

It is noticeable that the more sample is used for fabricating the database, the more accurate the prediction model will be. The experimental data show that when the sample size is 101, MRE and MAPE are 12.96 and 4.71 %, respectively, and when the sample size is 134, these two parameters are 12.85 and 4.65 %, respectively. It can be seen

Table 2 Part of the training sample data

Index	F_1	F_2	F_3	F_4	F_5	F_6	S_a/μm
1	0.967303	1.134019	0.001353	0.370379	0.009591	5,655.893	0.466
2	0.967668	1.157221	0.001038	0.342733	0.006703	5,603.668	0.493
3	0.96183	1.205407	0.000812	0.327822	0.003947	5,796.039	0.503
4	0.976033	1.154919	0.000729	0.333582	0.004883	6,465.93	0.525
5	0.963719	1.113795	0.001227	0.37771	0.006602	5,211.222	0.533
6	0.95422	1.20021	0.000759	0.331804	0.002843	6,896.375	0.548
7	0.975137	1.094622	0.000952	0.362857	0.006389	5,295.035	0.561
8	0.944366	1.212174	0.00058	0.290234	0.002497	2,820.967	0.573
9	0.96204	1.165633	0.000791	0.317963	0.002427	3,771.305	0.580
10	0.948574	1.091682	0.001097	0.340846	0.003802	2,024.794	0.585

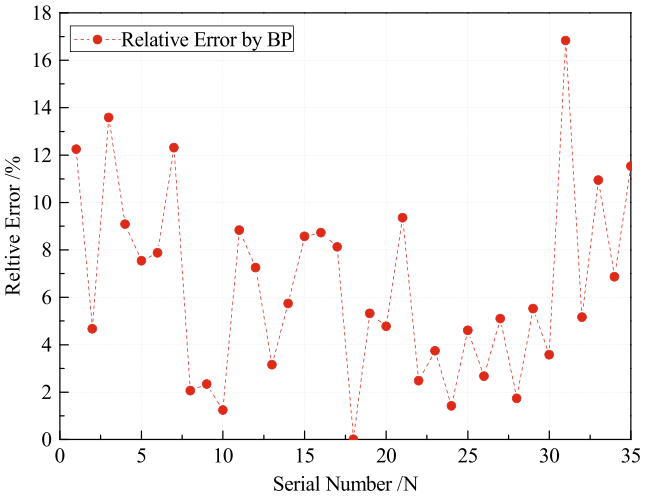

Fig. 11 Relative error for the BP model

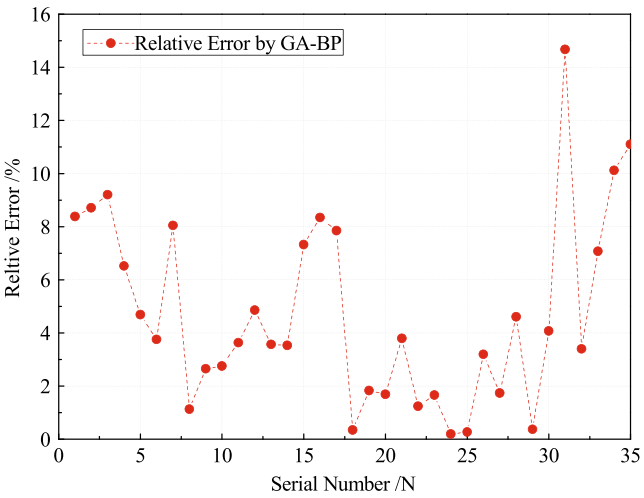

Fig. 13 Relative error for the GA-BP model

from the results that when the number of samples reaches more than 100, an increase in the number of samples has a little effect on accuracy. Meanwhile, due to the restriction of the number of parts, we only measure 134 pictures of 23 samples captured by the image acquisition system to create predictive models.

Based on these microscopic images, when MRE and MAPE, which illustrate the deviation between the actual value and the estimated one, reach the minimum simultaneously, the penalty factor C and sensitive coefficient ε can be confirmed. Based on the results of the experiment, the optimal parameters are found to be $C = 50$ and $\varepsilon = 0.07$. Consequently, the optimized SVM model is achieved.

5.2 Analysis of estimation results

In this paper, the proposed GLCM-SVM estimation model is testified by another new 35 sets of experimental data. Besides, the estimation accuracy of GLCM-SVM model is compared with the BP and GA-BP models. Based on the results of our past work, for both the BP and GA-BP models, the node number of the input layer, hidden layer, and output layer is 6, 15, and 1, respectively. Besides, for the GA-BP model, the population size is 30, intercrossing rate is 0.7, and mutating rate is 0.08.

Figures 10, 11, 12, 13, 14, and 15 show the comparison between the predictive values and the actual ones of surface roughness and the relative error of the BP, GA-BP, and SVM estimation models, respectively. As shown in Figs. 10 and 11, the MAE of the BP model is 0.107 μm, MRE is 16.83 %, and RMSE is 0.043 μm. Besides, as shown in Figs. 12 and 13, the MAE of the GA-BP model is 0.093 μm, MRE is 14.68 %, and RMSE is 0.039 μm. Moreover, MAPE of the BP and GA-BP models reach 6.43 and 4.75 %, respectively.

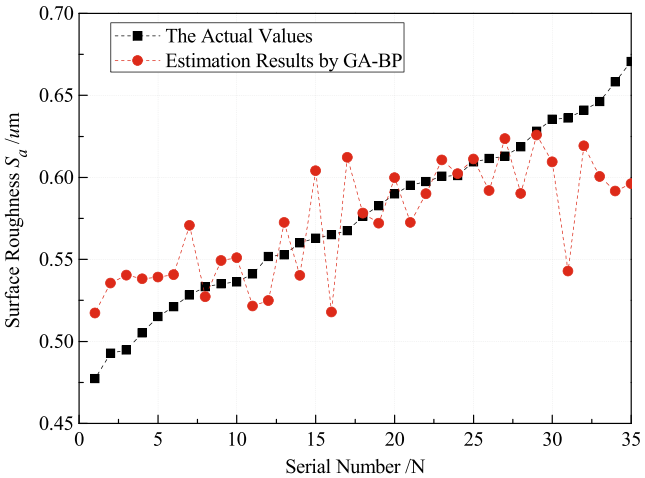

Fig. 12 Estimation results of the GA-BP model

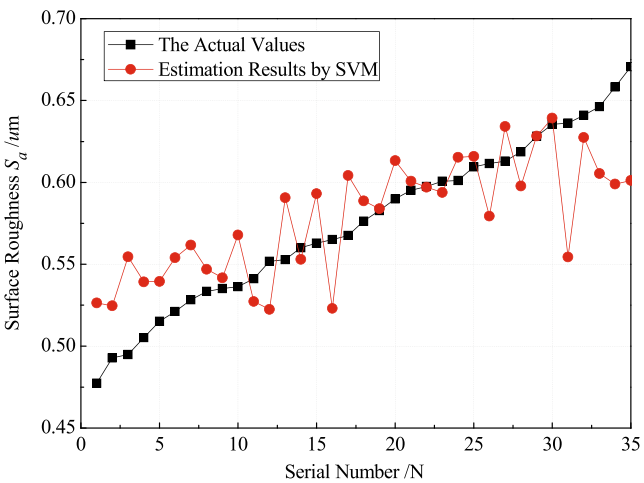

Fig. 14 Estimation results of the SVM model

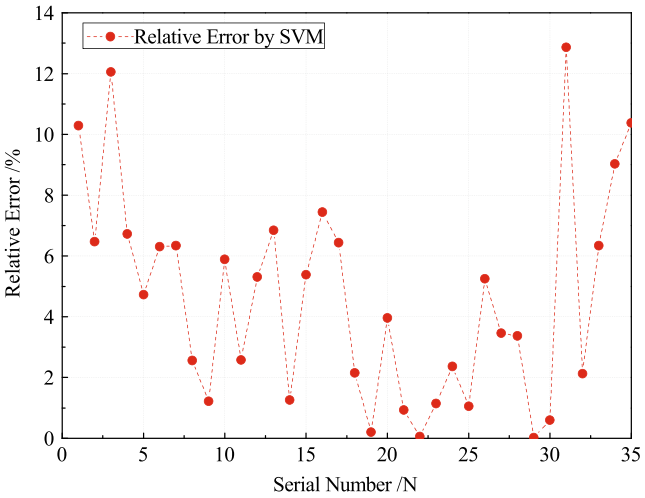

Fig. 15 Relative error for the SVM model

For the GLCM-SVM estimation model, as shown in Figs. 14 and 15, the MAE is 0.082 μm, MRE is 12.85 %, and RMSE is 0.033 μm. Moreover, MAPE of the GLCM-SVM estimation model reaches 4.65 %, which is smaller than that of both the BP and GA-BP models.

According to the experimental results and the estimation values from Figs. 14 to 15, MAPE of estimation values of the GLCM-SVM model is the smallest. There are only four groups of data, which have a relative error of more than 10 %. Meanwhile, there are 30 groups of data, which have a relative error of less than 8 %. Comparatively, as shown in Figs. 10, 11, 12, and 13, in the BP and GA-BP models, there are 12 groups and 8 groups of the estimation values, which have a relative error of more than 8 %. Moreover, the computation speeds for predicting the 35 sets of experimental data using the three predicted models are all fast enough. The computation time by means of BP and GA-BP is almost the same at 0.006 s, and it takes 0.05 s to predict the 35 sets of experimental data by using the SVM model (computer: Intel Processor 3.10 GHz, RAM memory 1.88 G). Therefore, the analysis above indicates that the proposed GLCM-SVM model has a higher estimation accuracy, is robust, has fast computing speed, and can be employed to access the surface roughness of R-surface in deep-hole valve. The results of the comparison made with the BP, GA-BP, and SVM models are illustrated in Table 3.

Table 3 The results of the comparison made with the BP, GA-BP, and SVM models

	MAPE (%)	MRE (%)	RMSE (μm)	MAE (μm)
BP	6.43	16.83	0.043	0.107
GA-BP	4.75	14.68	0.039	0.093
SVM	4.65	12.85	0.033	0.082

6 Conclusions

In this paper, an improved method based on microscopic vision to detect the surface roughness of R-surface in the valve is proposed. A hybrid GLCM-SVM roughness estimation model of R-surface is fabricated by employing GLCM and SVM algorithm. Moreover, the results of the experimental tests show that the proposed roughness estimation method based on the GLCM-SVM model exhibits higher estimation accuracy and generalization ability, which indicates that it is practicable to evaluate the surface roughness of micro-heterogeneous texture in deep-hole parts.

Acknowledgments This work was supported by the Key Laboratory Opening Funding of Micro-Systems and Micro-Structures Manufacturing of Ministry of Education, Harbin Institute of Technology (grant no. HIT. KLOF.2009002) and supported in part by the State Key Program of National Natural Science of China (grant no. 50835001).

References

1. Ghassan A, Kindi AL, Shirinzadeh B (2007) An evaluation of surface roughness parameters measurement using vision-based data. Int J Mach Tools Manufac 47:697–708
2. Shahabi HH, Ratnam MM (2010) Noncontact roughness measurement of turned parts using machine vision. Int J Adv Manuf Technol 46:275–284
3. Zhang JG, Tan TN (2002) Brief review of invariant texture analysis methods. Pattern Recognit 35:735–747
4. Tsai DM, Chen JJ, Chen JF (1998) A vision system for surface roughness assessment using neural networks. Int J Adv Manuf Technol 14:412–422
5. Lee KC, Ho SJ, Ho SY (2005) Accurate estimation of surface roughness from texture features of the surface image using an adaptive neuron-fuzzy inference system. Precis Eng 29:95–100
6. Hu ZX, Zhu L, Teng JX, Ma XH, Shi XJ (2009) Evaluation of three-dimensional surface roughness parameters based on digital image processing. Int J Adv Manuf Technol 40:342–348
7. Liu W, Zheng XY, Liu SJ, Jia ZY (2012) A roughness measurement method based on Genetic algorithm and neural network for microheterogeneous surface in deep-hole parts. J Circuit Syst Comput 21:125005–1250018
8. Dutta S, Datta A, Das Chakladar N, Pal SK, Mukhopadhyay S, Sen R (2012) Detection of tool condition from the turned surface images using an accurate grey level co-occurrence technique. Precis Eng 36:458–466
9. Alegre E, Barreiro J, Alexci SC (2012) A new improved Laws-based descriptor for surface roughness evaluation. Int J Adv Manuf Technol 59:605–615
10. Gadelmawla ES (2004) A vision system for surface roughness characterization using the gray level co-occurrence matrix. NDT&E Int 37:577–588
11. Xian GM (2010) An identification method of malignant and benign liver tumors from ultrasonography based on GLCM texture features and fuzzy SVM. Exp Syst Appl 37:6737–6741
12. Yang SH, Natarajan U, Sekar M, Palani S (2010) Prediction of surface roughness in turning operations by computer vision using

neural network trained by differential evolution algorithm. Int J Adv Manuf Technol 51:965–971
13. Wang PD, Meng QF, Zhao J, Li JJ, Wang XF (2011) Prediction of machine tool condition using support vector machine. 9th international conference on damage assessment of structures (DAMAS). J Phys Conf Ser 305:0121
14. Cao ZK, Han H, Gu B, Ren N (2009) A novel prediction model of frost growth on cold surface based on support vector machine. Appl Therm Eng 29:2320–2326
15. Zhang D, Sui WT (2011) The application of AR model and SVM in rolling bearings condition monitoring. Adv Res Comput Sci Inform Sci 152:326–331
16. Huang JD, Wang LS, Li GF, Zhang XZ, Wang JZ (2010) Prediction system of surface roughness based on LS-SVM in cylindrical longitudinal grinding. Optics Precis Eng 18(11):2407–2412
17. Lela B, Bajić D, Jozić S (2009) Regression analysis, support vector machines, and Bayesian neural network approaches to modeling surface roughness in face milling. Int J Adv Manuf Technol 42:1082–1088
18. Ekici S, Çaydas U (2010) Support vector machines models for surface roughness prediction in CNC turning of AISI 304 austenitic stainless steel. J Intell Manuf 23:639–650
19. Vapnik VN (1998) Statistical learning theory. Wiley, New York